RESEARCH ARTICLE

Key Points:
- Water vapor displays structured absorption bands over the 290- to 350-nm range, with cross sections in the range of 10^{-24} to 10^{-25} cm^2/molecule
- Field evidence for water vapor near-UV absorption is presented
- Water vapor near-UV absorption affects O$_3$ retrieval and modeling of atmospheric radiation and climate

Supporting Information:
- Supporting Information S1

Correspondence to:
L. Zhu,
lei.zhu@health.ny.gov

Water Vapor Near-UV Absorption: Laboratory Spectrum, Field Evidence, and Atmospheric Impacts

Linsen Pei[1,2], Qilong Min[3], Yuyi Du[3], Zhechen Wang[1], Bangsheng Yin[3], Kai Yang[4], Patrick Disterhoft[5], Thomas Pongetti[6], and Lei Zhu[1,7]

[1]Wadsworth Center, New York State Department of Health, Albany, NY, USA, [2]Now at Selected Lab Partners, Greensboro, NC, USA, [3]Atmospheric Sciences Research Center, University at Albany, Albany, NY, USA, [4]Department of Atmospheric and Oceanic Science, University of Maryland, College Park, MD, USA, [5]NOAA Earth System Research Laboratory Global Monitoring Division, Boulder, CO, USA, [6]Jet Propulsion Laboratory, California Institute of Technology, Pasadena, CA, USA, [7]Department of Environmental Health Sciences, University at Albany, Albany, NY, USA

Abstract Absorption of solar radiation by water vapor in the near-UV region is a poorly understood but important issue in atmospheric science. To better understand water vapor near-UV absorption, we constructed a cavity ring-down spectrometer with bandwidth of 5 cm^{-1} (~0.05 nm) and obtained water vapor absorption cross sections at 1-nm increments in the 290- to 350-nm region. Water vapor displays structured absorption over this range with maximum and minimum cross sections of 8.4×10^{-25} and 1.6×10^{-25} cm^2/molecule. Major water vapor absorption bands were observed at 293–295, 307–313, 319, 321–322, and 325 nm, with cross-section values higher than 4.0×10^{-25} cm^2/molecule. To obtain further insight into major water vapor absorption bands, we measured water vapor absorption cross sections at 0.05-nm intervals in the 292- to 296-nm, 306- to 314-nm, and 317- to 326-nm region. Field UV residual spectra not only exhibited increased attenuation at higher atmospheric water vapor loadings but also showed structures suggested by the laboratory water vapor absorption spectrum. Spaceborne UV radiance spectra have spectral structures resembling the differential cross-section spectrum constructed from the laboratory wavelength-dependent water vapor absorption cross sections presented here. Incorporating water vapor absorption cross-section data into a radiative transfer model yielded an estimated energy budget of 0.26 W/m^2 for the standard U.S. atmosphere and 0.76 W/m^2 for the tropics. This shows that water vapor near-UV absorption is an important contributor for climate simulation and ozone retrievals.

Plain Language Summary Water vapor near-UV absorption is an overlooked subject of core importance to atmospheric science. We constructed a cavity ring-down spectrometer with a bandwidth comparable to those of field UV spectrometers and determined water vapor absorption cross sections at 1-nm intervals in the 290- to 350-nm region. We also measured water vapor absorption cross sections at 0.05-nm intervals surrounding major absorption bands. We provide field evidence to support laboratory water vapor near-UV absorption measurements and present comparisons of the estimated optical depth spectra of ozone with those of water vapor for the standard U.S. and tropical atmospheres. Our findings suggest that water vapor near-UV absorption will significantly affect ozone retrieval from UV measurements, particularly in the tropical region. Incorporating cross-section data into a radiative transfer model, we estimated that the energy budget of water vapor near-UV absorption was about 0.26 W/m^2 for the standard U.S. atmosphere and 0.76 W/m^2 for the tropics. Since it was not thought that water vapor could have near-UV absorption, the effect of such absorption is not currently included in radiation and climate simulation models. Our work on water vapor near-UV absorption is expected to change the paradigm in atmospheric measurements from UV remote sensing observations and how atmospheric radiation and climate are modeled.

1. Introduction

Water vapor is a strong IR absorber (Rothman et al., 2009; Tennyson et al., 2013) and plays a dominant role in the radiative balance of the atmosphere (Bernath, 2002; Houghton et al., 2001). However, water vapor absorption in the near-UV region and the impact of such absorption on ozone retrieval and atmospheric radiation budget is much less understood, due to theoretical and experimental challenges. Recent advances in theoretical and experimental techniques have made it possible to tackle overarching research topics of water vapor near-UV absorption and its atmospheric impacts. Theoretical calculations (Choi & Light, 1992; Császár et al., 2010; Li & Guo, 2001; Mussa & Tennyson, 1998; Tennyson, 2014) and multiphoton

excitation studies (Grechko et al., 2008; Maksyutenko et al., 2007) have attributed water vapor absorption in the 290- to 350-nm region (i.e., 34482.759–28571.429 cm^{-1}) to vibration overtone and combination bands containing at least nine quanta of excitation. There are 268 predicted vibrational bands for water vapor in the 290- to 350-nm region (Császár et al., 2010), with extensive state mixings. Makogon et al. (2013) reported increased photo-acoustic signal magnitude when a mixture of water vapor and nitrogen was irradiated with 266-nm radiation at higher water vapor partial pressures. We conducted the first experimental study (Du, Huang, Min, & Zhu, 2013) demonstrating water vapor to have single-photon near-UV absorption in the 290- to 350-nm range using a sensitive absorption technique, cavity ring-down spectroscopy (O'Keefe et al., 1990; O'Keefe & Deacon, 1988). By using a narrow linewidth (0.15 cm^{-1}) dye laser, water vapor absorption cross sections with values ranging from 2.9×10^{-24} to 2.1×10^{-25} cm^2/molecule were obtained at 5-nm intervals (Du, Huang, Min, & Zhu, 2013). Subsequently, Wilson et al. (2016) used incoherent broadband cavity-enhanced absorption spectroscopy to measure water vapor near-UV absorption in an environmental chamber containing NO_2 and HONO. They did not detect water vapor near-UV absorption and gave an upper limit to water vapor absorption cross section of 5×10^{-26} cm^2/molecule. Wilson et al. used cavity mirrors with a maximum reflectivity of 99.3% (minimum transmission loss of 7,000 ppm per mirror) in the near-UV region. Such a setup has an estimated detection sensitivity of 140 ppm per round trip, assuming 1% error in cavity loss measurement (with a well-aligned cavity, 1% error is typical for exponential fitting of decay curves with many averages). Therefore, with 10-Torr water vapor in a 4.1-m-long cavity, the lowest water vapor absorption cross section Wilson et al. could theoretically measure would seem to be $\sim 5 \times 10^{-25}$ cm^2/molecule, rather than 5×10^{-26} cm^2/molecule as reported. Since the signal size needs to be several times the detection sensitivity to obtain a reliable absorption measurement, we assert that the system used by Wilson et al. did not have enough sensitivity to detect the weak water vapor near-UV absorptions reported here.

Water vapor is widely abundant in the lower troposphere, with a concentration of up to 5 orders of magnitude higher than that of ozone in the lower atmosphere. With near-UV absorption cross sections on the order of 10^{-25} to 10^{-24} cm^2/molecule, the attenuation effect of water vapor on near-UV radiation could be significant, particularly in the tropical environment. Not accounting for near-UV absorption by water vapor could lead to overestimation of ozone amount and to reduction of accuracy in satellite UV ozone measurements. This can ultimately lead to erroneous assessment of long-term ozone trend. Furthermore, water vapor near-UV absorption may significantly impact the modeling of near-UV solar radiation on the ground. However, water vapor near-UV absorption has so far not been included in the modeling of near-UV radiative flux at the Earth's surface. Unlike the ozone absorption, which happens primarily in the upper atmosphere, water vapor absorption mostly occurs in the lower atmosphere, which will impact the climate system significantly and differently.

Water vapor absorption in the 290- to 350-nm region has so far not been reported in the Earth's atmosphere. A field-compatible laboratory water vapor near-UV absorption spectrum is necessary to guide such detection. While our previous proof-of-concept study (Du, Huang, Min, & Zhu, 2013) illustrated the potential importance of water vapor near-UV absorption on near-UV radiative flux at the ground, the narrow line-width dye laser employed in that study was not compatible in spectral resolution with field UV instruments (several cm^{-1} to tens of cm^{-1}). Since the nature of the water vapor near-UV absorption band is that of highly excited vibrational transitions, spectral shape and cross-section values are likely dependent upon wavelength resolution of the probe system and at what wavelength interval water vapor near-UV absorption is sampled.

In this paper, we report the first field-compatible water vapor near-UV absorption spectrum obtained using cavity ring-down spectroscopy with 5 cm^{-1} bandwidth. We determined room temperature (295 ± 1 K) water vapor absorption cross sections at 1-nm increments over the 290- to 350-nm range. Over the 292- to 296-nm, 306- to 314-nm, and 317- to 326-nm region where major water vapor absorption bands were observed, we obtained water vapor absorption cross sections at 0.05-nm intervals. Analyses of residuals from ground-based and satellite near-UV spectra are presented, which have provided field evidence for water vapor near-UV absorption. We use an atmospheric radiative transfer model to evaluate the effect of water vapor near-UV absorption on modeled solar irradiance at the ground and discuss the atmospheric impacts of the results.

2. Materials and Methods

2.1. Laboratory Water Vapor Near-UV Absorption Measurements

A laboratory water vapor near-UV spectroscopic study was conducted at the Wadsworth Center. A cavity ring-down spectrometer equipped with a broadband probe laser source (about 5 cm^{-1} bandwidth) was constructed to measure water vapor near-UV absorption cross sections. The probe laser system was the frequency-doubled output of a Spectra Physics optical parametric oscillator pumped by the third harmonic of a Nd:YAG laser. The tunable UV probe beam was collimated by irises and directed into a 99-cm long ring-down cavity vacuum sealed with a pair of highly reflective cavity mirrors. A tiny fraction of the probe beam entered the cavity through the front mirror. The trapped probe beam decayed due to mirror transmission loss as well as absorption and scattering of the probe beam by water vapor inside the cavity. The probe light that leaked from the end mirror of the cavity was detected by a photomultiplier tube (PMT). The output of the PMT was preamplified, digitized, and sent to a computer for processing. The decay profile was fitted with a single-exponential decay function to calculate the total loss (Γ) per round-trip pass.

The liquid water sample that was used in the current study was quadruply distilled water from a glass distiller using building deionized water as input. Trace volatile impurity in the distilled water sample was determined using EPA 8260 purge-and-trap method followed by gas chromatography-mass spectrometry analysis. The only impurity that was detected was ~3-ppb acetone (mole ratio) in distilled water. Based upon estimates found in the literature for near-UV absorption cross sections of acetone (Atkinson et al., 1997), the determined acetone impurity, the vapor pressures of acetone and water at room temperature (Lide, 2008), water vapor pressure used, and cavity length, we conclude that the acetone vapor had negligible interference in the water vapor near-UV absorption measurement.

Distilled water in a glass bulb was purified by repeated freeze-pump-thaw cycles to remove dissolved gases and was further pumped prior to each experiment before water vapor was introduced into the gas cell. The stainless-steel gas cell was newly constructed. It was cleaned with acetone and methanol, and subsequently heated and pumped extensively with a pumping system consisting of a rotary pump and a diffusion pump to ensure that the chamber wall was clean. The background vacuum of the cell was around 2×10^{-6} Torr, monitored by a cold cathode ion gauge. The water vapor pressure used in the extinction cross-section measurement ranged from 1 Torr (1.3×10^2 Pa) up to about 10 Torr (1.3×10^3 Pa). Water vapor pressure inside the cell was monitored by a capacitance manometer, with a maximum scale of 100 Torr and measurement uncertainty of less than 0.25%. Absorption and scattering of the near-UV laser beam by water vapor was measured under static conditions at an ambient temperature of 295 ± 1 K.

2.2. Residual Analysis Method for Field UV Spectra

Atmospheric near-UV-absorbing gases such as O_3, SO_2, water vapor, formaldehyde (H_2CO), and NO_2, as well as aerosol extinction and Rayleigh scattering, can affect solar irradiance in the UV spectral region between 290 and 350 nm under clear-sky condition. The concentration of NO_2 was low and its effects on surface radiation were negligible in our analysis. To investigate possible near-UV absorption by water vapor, we examined residuals of field UV spectra by subtracting the fitted optical depths by Rayleigh scattering, aerosol extinction, and absorption by O_3 and SO_2 from the measured total optical depth for the whole atmosphere. The relationship between total optical depth and optical depths of Rayleigh, aerosol, O_3, SO_2, and residual can be approximated using the equation given by Min and Harrison (1998):

$$\tau = \tau_{\text{Ray}} + \sum_{i=0}^{4} x_i \left(\frac{1}{\lambda}\right)^i + K^{O3}(\lambda)\left(x_5 + x_6\left(\frac{1}{\lambda}\right)\right) + K^{SO2}(\lambda)\left(x_7 + x_8\left(\frac{1}{\lambda}\right)\right) + \text{residual} \tag{1}$$

where τ represents total optical depth for the whole atmosphere, the first to fifth terms on the right-hand side of equation (1) represent respective contribution to optical depth by Rayleigh, aerosol, O_3, SO_2, and residual. In equation (1), x_1-x_4 are coefficients related to aerosols, x_5 and x_6 are those related to the amount of O_3, x_7 and x_8 are those related to the amount of SO_2, $K^{O3}(?)$ and $K^{SO2}(?)$ represent absorption spectra of O_3 and SO_2 at a given temperature, and ? is wavelength in micrometer unit. Equation (1) holds for the direct and the diffuse radiation. Coefficients x_6 and x_8 will be equal to zero when the direct solar beam is used. The contribution of Rayleigh scattering can be calculated using equation (2) below:
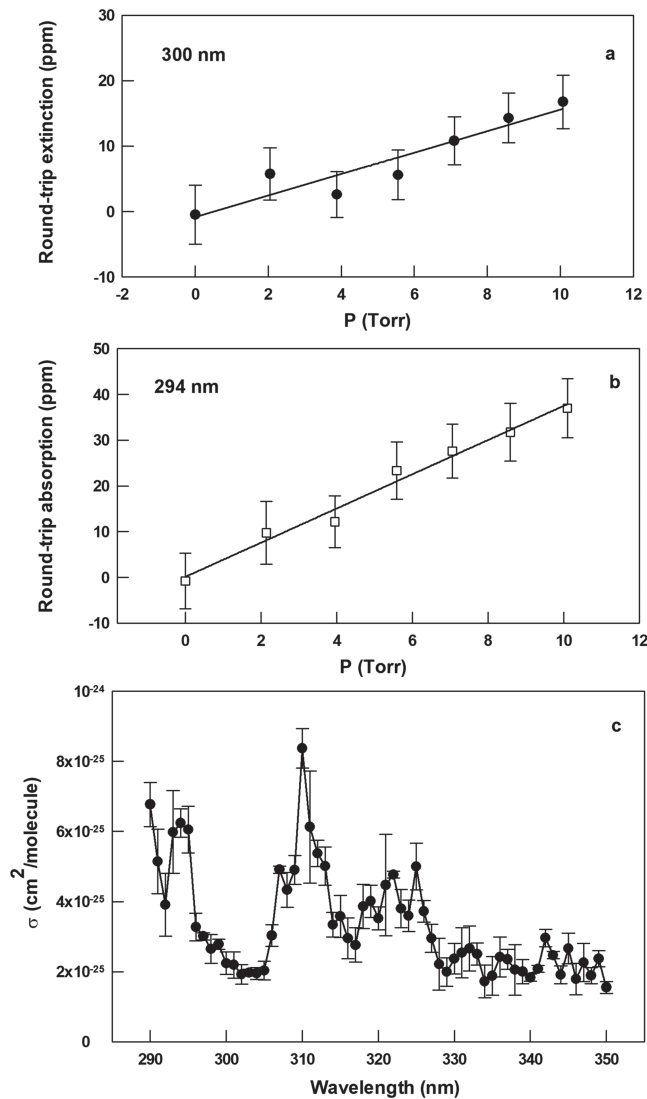
Figure 1. (a) Round-trip extinction at 300 nm as a function of the H_2O pressure. A linear least squares analysis of the experimental data is shown as a solid line. (b) Round-trip absorption at 294 nm as a function of the H_2O pressure, along with linear least squares analysis of the results. (c) Gas phase H_2O absorption cross sections at 1-nm intervals over the 290- to 350-nm range.

$$\tau_{Ray} = 0.008569\lambda^{-4}\left(1 + 0.0113\lambda + 0.00013\lambda^2\right)\frac{P}{P_0} \qquad (2)$$

where P and P_0 are pressures at the measurement site and at the sea level (Hansen & Travis, 1974). By subtracting the contribution to the optical depth spectra by SO_2, O_3, Rayleigh scattering, and aerosol extinction from the total optical depth spectra, we obtained residuals attributable to the optical depths (air masses, AMs) of water vapor and formaldehyde for a given zenith angle. Water vapor and formaldehyde are spectrally separated in the 306- to 314-nm range, as shown in section 3.

2.3. Spaceborne Spectral Measurements

The Ozone Monitoring Instrument (OMI) (Levelt et al., 2006) onboard the National Aeronautics and Space Administration's Aura satellite has provided Earthshine measurements between 260 and 500 nm since October 2004. These spectral measurements sample a wide range of atmospheric water vapor loadings as the satellite orbits around the Earth and delivers daily global observational coverage. We applied the iterative spectral fitting algorithm (Yang et al., 2009) to retrieve O_3 and other trace gases (such as SO_2) from OMI spectral measurements and compared fitting residuals (e.g., Figure 2 in Yang et al., 2009) under different observational conditions. We also used Modern-Era Retrospective analysis for Research and Applications, Version 2 (MERRA-2) data to estimate the total water vapor vertical column for OMI observations.

3. Results and Discussion

3.1. Laboratory Water Vapor Near-UV Absorption Spectrum at 295 K

3.1.1. Water Vapor Absorption Spectrum at 1-nm Interval Over 290- to 350-nm Range

We measured water vapor extinction (absorption + scattering) cross sections at 1 nm increments over the 290- to 350-nm range using cavity ring-down spectroscopy with a cavity length of 99 cm. The extinction cross section was obtained by fixing the laser at a specific wavelength and recording the round-trip extinction by water vapor as a function of its pressure. Several sets of highly reflective cavity mirrors (mirror transmission loss in the range of 300–2000 ppm per mirror, with higher cavity loss at shorter wavelengths) were used to ensure we had enough sensitivity to detect weak water vapor near-UV extinction. Figure 1a illustrates round-trip extinction as a function of water vapor pressure at 300 nm, which shows extinction increasing as water vapor pressure rises in the 1- to 10-Torr range. About 20 repeated measurements were made at each pressure, and each measurement was the average of 50 ring-down curves (or about 10 repeated measurements were made at each pressure and each measurement was the average of 100 ring-down curves). The average value of the repeated measurement was used for the analysis. By fitting the experimental data to a linear plot, we acquired a water vapor extinction cross section of 2.6×10^{-25} cm²/molecule at 300 nm. Water vapor scattering cross-sections range from 6.5×10^{-27} to 5.9×10^{-27} cm²/molecule within the 290–350 nm range (see Figure 1 in Sutton & Driscoll, 2004), being about 6.4×10^{-27} cm²/molecule at 300 nm. We derived a water vapor absorption cross section of 2.6×10^{-25} cm²/molecule at 300 nm, which is about 40 times greater than its scattering cross section. The absorption cross-section value reported here at 300 nm is smaller than that of $(8.7 \pm 0.3) \times 10^{-25}$ cm²/molecule obtained in our previous work (Du, Huang, Min, & Zhu, 2013), where the error quoted represents 1σ measurement error. Distilled and degassed water was used as the source of water vapor in this study, while triply deionized and
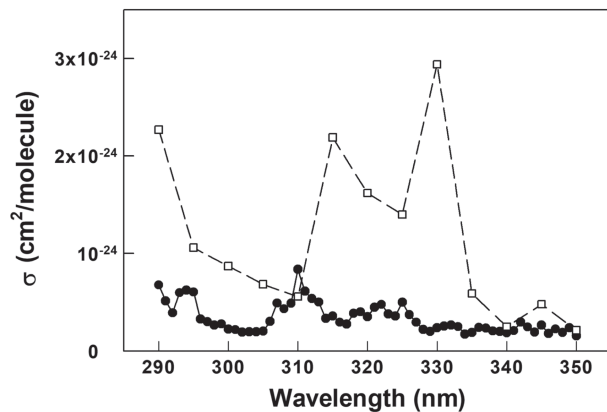
Figure 2. Comparison between gas phase H_2O absorption cross sections over the 290- to 350-nm range determined in this work (circles) and those data (squares) obtained by Du, Huang, Min, and Zhu (2013).

degassed water was used in the Du, Huang, Min, and Zhu study (2013). As water vapor near-UV absorption is weak, and a tiny amount of UV-absorbing impurity could increase the absorption cross-section value, we conducted water vapor absorption cross-section measurements at 300 nm under the same conditions, varying only the sources of liquid water used to draw water vapor. The absorption cross-section value at 300 nm for water vapor drawn from triply deionized water was about 2.2 times that for water vapor drawn from distilled water, suggesting that a trace amount of UV-absorbing impurity is present in the triply deionized water. Anion chromatogram analysis showed the presence of about 27 ppb (mole ratio) of nitrate ion (NO_3^-), about 7 ppb of chloride ion, and an unknown peak likely associated with small amount of formate ion ($HCOO^-$), acetate ion (CH_3COO^-), propionate ion ($C_2H_5COO^-$), and fluoride ion (F^-) in triply deionized water. Near-UV-absorbing impurity such as nitrate-water clusters could be introduced into the gas phase and detected by the ring-down probe beam. This is one likely reason why Du and colleagues' (2013) water vapor near-UV absorption cross sec-

tions were larger than those obtained in our current study, as they used triply deionized water as the source of water vapor, while quadruply distilled water in a glass distiller was used as the source of water vapor in our current study. The difference in laser wavelength resolution used in the present (5 cm^{-1}) and the previous (0.15 cm^{-1}) work may have further contributed to the difference in the cross-section values. At the

beginning of the current study, we also determined water vapor absorption cross section at 300 nm using a 50-cm long cavity and compared results with that obtained using a 99-cm long cavity, observing that the measured absorption values at a given water vapor pressure increased linearly with cavity length. We obtained similar absorption cross-section values using 50- and 99-cm long cavities, suggesting that what we measured indeed came from water vapor absorption in the gas phase. Unpublished results of the Zhu group have shown peak water vapor near-UV absorption cross sections over the 290- to 350-nm range to increase with temperature in the 283- to 333-K range, which again is consistent with water vapor near-UV absorption in the gas phase. We determined background cavity losses before we introduced water vapor into the cavity and before we varied water vapor pressure inside the cavity. We found no evidence for water vapor adsorption on cavity mirrors in the water vapor pressure range (1–10 Torr) used in the cross-section determination, perhaps because the cavity mirrors were superpolished. In a prior study targeted at investigating water vapor adsorption on fused silica windows (Du, Huang, & Zhu, 2013), we found water vapor adsorption on cavity mirrors only occurred at 294 K when its pressure inside the cavity was about 15 Torr or higher.

To avoid interference from a trace amount of UV-absorbing impurity in triply deionized water, we conducted all water vapor absorption cross-section measurements using distilled water as the source of water vapor. Displayed in Figure 1b is absorption as a function of water vapor pressure for 294 nm. A linear least squares analysis of the data yields a corresponding cross-section value of 5.8×10^{-25} cm^2/molecule. Water vapor absorption cross-section values obtained in this study in the 290- to 350-nm region are listed in Table 1 and plotted in Figure 1c. As seen from Figure 1c, water vapor displayed a structured absorption spectrum in the 290- to 350-nm region, with maximum and minimum absorption cross sections of $(8.4 \pm 0.6) \times 10^{-25}$ and $(1.6 \pm 0.2) \times 10^{-25}$ cm^2/molecule, where errors quoted represent 1σ scatter of repeated measurement

Table 1
Gas Phase Absorption Cross Sections of H_2O Vapor at 1-nm Intervals in the 290–350 nm Range

λ (nm)	σ (cm^2/molecule)	λ (nm)	σ (cm^2/molecule)
290	$(6.8 \pm 0.7) \times 10^{-25}$	321	$(4.5 \pm 1.5) \times 10^{-25}$
291	$(5.1 \pm 1.0) \times 10^{-25}$	322	$(4.8 \pm 0.1) \times 10^{-25}$
292	$(3.9 \pm 0.9) \times 10^{-25}$	323	$(3.8 \pm 0.6) \times 10^{-25}$
293	$(6.0 \pm 1.2) \times 10^{-25}$	324	$(3.6 \pm 0.5) \times 10^{-25}$
294	$(6.2 \pm 0.5) \times 10^{-25}$	325	$(5.0 \pm 0.7) \times 10^{-25}$
295	$(6.1 \pm 0.7) \times 10^{-25}$	326	$(3.7 \pm 0.4) \times 10^{-25}$
296	$(3.3 \pm 0.4) \times 10^{-25}$	327	$(3.0 \pm 0.4) \times 10^{-25}$
297	$(3.0 \pm 0.1) \times 10^{-25}$	328	$(2.2 \pm 0.8) \times 10^{-25}$
298	$(2.7 \pm 0.5) \times 10^{-25}$	329	$(2.0 \pm 0.5) \times 10^{-25}$
299	$(2.8 \pm 0.2) \times 10^{-25}$	330	$(2.4 \pm 0.5) \times 10^{-25}$
300	$(2.2 \pm 0.4) \times 10^{-25}$	331	$(2.5 \pm 0.8) \times 10^{-25}$
301	$(2.2 \pm 0.4) \times 10^{-25}$	332	$(2.7 \pm 0.7) \times 10^{-25}$
302	$(1.9 \pm 0.3) \times 10^{-25}$	333	$(2.5 \pm 0.4) \times 10^{-25}$
303	$(2.0 \pm 0.1) \times 10^{-25}$	334	$(1.7 \pm 0.5) \times 10^{-25}$
304	$(2.0 \pm 0.2) \times 10^{-25}$	335	$(1.9 \pm 0.6) \times 10^{-25}$
305	$(2.0 \pm 0.3) \times 10^{-25}$	336	$(2.4 \pm 0.6) \times 10^{-25}$
306	$(3.0 \pm 0.4) \times 10^{-25}$	337	$(2.4 \pm 0.3) \times 10^{-25}$
307	$(4.9 \pm 0.1) \times 10^{-25}$	338	$(2.1 \pm 0.8) \times 10^{-25}$
308	$(4.3 \pm 0.5) \times 10^{-25}$	339	$(2.0 \pm 0.4) \times 10^{-25}$
309	$(4.9 \pm 0.5) \times 10^{-25}$	340	$(1.8 \pm 0.1) \times 10^{-25}$
310	$(8.4 \pm 0.6) \times 10^{-25}$	341	$(2.1 \pm 0.1) \times 10^{-25}$
311	$(6.1 \pm 1.6) \times 10^{-25}$	342	$(3.0 \pm 0.3) \times 10^{-25}$
312	$(5.4 \pm 0.4) \times 10^{-25}$	343	$(2.5 \pm 0.1) \times 10^{-25}$
313	$(5.0 \pm 0.6) \times 10^{-25}$	344	$(1.9 \pm 0.3) \times 10^{-25}$
314	$(3.3 \pm 0.4) \times 10^{-25}$	345	$(2.7 \pm 0.5) \times 10^{-25}$
315	$(3.6 \pm 0.6) \times 10^{-25}$	346	$(1.8 \pm 0.5) \times 10^{-25}$
316	$(3.0 \pm 0.6) \times 10^{-25}$	347	$(2.3 \pm 0.6) \times 10^{-25}$
317	$(2.8 \pm 0.5) \times 10^{-25}$	348	$(1.9 \pm 0.3) \times 10^{-25}$
318	$(3.9 \pm 0.7) \times 10^{-25}$	349	$(2.4 \pm 0.3) \times 10^{-25}$
319	$(4.0 \pm 0.5) \times 10^{-25}$	350	$(1.6 \pm 0.2) \times 10^{-25}$
320	$(3.5 \pm 0.4) \times 10^{-25}$		

Table 2
Vibrational Bands That May Have Contributed to the Water Vapor Major Absorption Peaks Shown in Figure 1c Based Upon Band Origin Assignments by Császár et al. (2010)

Vibrational band	Band origin wavelength (nm)	Vibrational band	Band origin wavelength (nm)
(1,20,0)	294.00	(6,2,3)	318.55
(7,2,3), (8,2,2)	295.06	(7,2,2)	318.60
(12,0,0), (11,0,1)	295.49	(1,17,1)	319.61
(7,1,3), (8,1,2)	307.08	(7,0,3), (8,0,2)	320.39
(9,2,1)	308.98	(2,17,0)	320.91
(10,2,0)	309.01	(3,3,5)	321.33
(5,2,4)	309.61	(4,3,4)	321.49
(1,19,0)	310.65	(9,1,1)	321.76
(6,0,4)	310.85	(10,1,0)	321.78
(5,0,5)	310.94	(4,1,5)	322.80
(0,1,9)	311.58	(5,1,4)	322.89
(0,19,1)	312.54	(0,20,0)	322.95
(11,0,0), (10,0,1)	313.31	(0,0,9)	325.49
(1,1,8)	313.56		

Note. $\nu 1$, $\nu 2$, $\nu 3$ are used to represent quantum numbers for the symmetric stretch, bend, and antisymmetric stretch vibrational normal modes ($\nu 1, \nu 2, \nu 3$) in water.

results. Over the 292- to 350-nm range, there were six major peaks with cross-section values larger than 4×10^{-25} cm^2/molecule; they were located at 293–295, 307–313, 319, 321–322, and 325 nm. Minor absorption peaks were observed at 315, 331–333, 336–337, 342, 345, 347, and 349 nm, with cross-section values between 2.2×10^{-25} and 4.0×10^{-25} cm^2/molecule. Császár et al. (2010) made theoretical vibrational quantum number assignments for water vapor highly excited stretch overtone and the combination bands. The vibrational bands that may have contributed to the observed major and minor absorption peaks are tabulated in Tables 2 and S1 in the supporting information. It should be noted that theoretical vibrational band origins have been calculated for $J = 0$ rotational levels. In our experiments, we detected water vapor near-UV absorption from a Boltzmann distribution of rotational states. Since the room temperature Boltzmann distribution of rotational states is expected to peak at higher rotational quantum numbers than $J = 0$, peak positions may be shifted between our observed absorption maxima and the calculated vibrational band origins.

In the wavelength range 290–299 nm, the water vapor spectrum appears to be on the tail of an absorption band. We speculate that the very long tail of the electronic absorption band of water vapor (Okabe, 1978) may have contributed to the downward slope of water vapor near-UV absorption over the 290- to 299-nm range. In our previous study, water vapor absorption cross section was sampled at 5-nm intervals over the 290- to 350-nm range and the continuum underneath the water vapor near-UV absorption band was minimally noticeable. The continuum feature below 300 nm was more noticeable when we made water vapor absorption cross-section measurements at 1-nm intervals.

We compared the water vapor near-UV absorption spectrum shown in Figure 1c to that obtained from our previous study (Du, Huang, Min, & Zhu, 2013). Both spectra are presented in Figure 2 for ease of viewing. More vibrational structures are apparent from the results of the current study, for number of reasons. While our prior study experimentally demonstrated that water vapor had single-photon near-UV absorption in the 290-350-nm region, that study had its limitations. Water vapor absorption spectrum shape, peak positions, and size can vary with the spectral resolution of the probing laser system and the frequency of sampling. The 5-nm sampling interval for water vapor near-UV absorption in our first study was not frequent enough to investigate its structured absorption bands, leading us to adjust the interval to 1 nm for the current study. As mentioned before, the spectral resolution of the narrow linewidth (0.15 cm^{-1}) dye laser available for our use at the time of the earlier study was much narrower than those of field UV instruments. Our previous study reported the highest water vapor absorption cross-section value of 2.9×10^{-24} cm^2/molecule at 330 nm, but we did not observe a major absorption band at this wavelength from the current study. We identified an approximately 27 ppb nitrate ion impurity in triply deionized water in our prior study, which may have contributed to the large water vapor absorption cross-section value observed at 330 nm. Nitrate ion on

surfaces has reported absorption cross-section values (Sangwan et al., 2016) of 1.6×10^{-19}, 2.4×10^{-19}, and 2.7×10^{-19} cm^2/molecule at 330, 335, and 340 nm, respectively. The spectrum of nitrate-water clusters might be blue shifted compared to that of nitrate ion on surfaces. Absorption by nitrate-water clusters may have contributed to the large 330-nm water vapor absorption cross section reported in our first study. Our previous study also used the frequency-doubled output of an excimer-pumped dye laser as the probe laser source for the cavity ring-down spectrometer at 330 nm and shorter wavelengths. The DCM laser dye used at 330 nm is known to be unstable. Although absorption of 330-nm light by water vapor was repeatedly measured many times at a given water vapor pressure, and such measurements were repeated at different water vapor pressures, the instability of the DCM laser dye may also have contributed to the large 330-nm water vapor absorption cross-section value reported in our previous study.

Lampel et al. (2015, 2017) observed a water vapor absorption band near 363 nm using field spectra obtained by differential optical absorption spectroscopy and using the POKAZATEL line list to identify absorption. With 0.5-nm spectral resolution, they gave maximum water vapor absorption cross section of 2.7×10^{-27} cm^2/molecule at 362.3 nm, and upper limit to water vapor absorption cross section of 1.4×10^{-26} cm^2/molecule in the 340- to 360-nm range. Our highest water vapor absorption cross section in the 340- to 350-nm range is ~3.0×10^{-25} cm^2/molecule, with a probe laser bandwidth of 5 cm^{-1} (~0.05 nm). The different spectral resolution used in the Lampel et al. study and the current work could result in differences in cross-section values. The full width at half maximum (FWHM) of the Voigt profile (f_V) of water vapor is estimated to be about 0.11 cm^{-1} at 340 nm, calculated using equation (3) below:

$$f_V \approx 0.5346 f_L + \left(0.2166 f_L{}^2 + f_G{}^2 \right)^{1/2} \qquad (3)$$

where f_L is the FWHM of the Lorentzian profile and f_G is the FWHM of the Gaussian profile. Since our probe laser bandwidth of 5 cm^{-1} is about 45 times that of the water vapor Voigt line broadening, we can provide vibrational band information of water vapor in the near-UV but cannot resolve individual ro-vibrational lines. The spectral resolution used by Lampel et al. would correspond to 43 cm^{-1} at 340 nm, which is about 391 times the Voigt line broadening of water vapor. Also, multiple species can absorb/scatter solar radiation in the 340- to 350-nm region in the field spectra. Any errors in the subtraction of individual components will affect the size of the field residuals. It is unknown to what extent the upper limit to the water vapor near-UV absorption cross section deduced by Lampel et al. might have been affected by uncertainty in the subtraction of individual components. It should be noted that our laboratory study was conducted only in the presence of water vapor and we measured water vapor absorption as a function of its pressure to obtain water vapor near-UV absorption cross sections.

We have compared the 1-nm interval water vapor near-UV absorption spectrum determined in this study to that calculated by Conway et al. (2018). Conway and colleagues created a global dipole moment surface for the ground electronic state of water and improved upon the accuracy in predicting transition strengths in the IR, visible, and at 363 and 377 nm. In the 290- to 350-nm region, they calculated ro-vibrational transitions at $J \leq 14$ and they predicted the peak cross section for an individual ro-vibrational line to be 7×10^{-27} cm^2/molecule. Since the water vapor near-UV absorption spectrum reported in this paper appears to be on the long tail of an electronic absorption band, particularly in the 290- to 299-nm region, the long tail electronic absorption band of water vapor may increase its vibrational transition strength in the 290- to 350-nm region. The effect of the long tail water vapor electronic absorption band on the vibrational transition strength in the near-UV is a subject worth exploring.

3.1.2. Water Vapor Spectrum at 0.05-nm Interval Surrounding Major Absorption Bands

To gain further insight into the absorption bands at 293–295, 307–313, 319, 321–322, and 325 nm, we determined water vapor absorption cross sections at 0.05-nm intervals over the 292- to 296-nm, 306- to 314-nm, and 317- to 326-nm region. There are twenty 0.05-nm intervals in 1 nm. To obtain water vapor absorption cross-section data at 0.05-nm intervals, we first determined the background cavity losses at the beginning of the 1-nm interval several times; we then sent a command to increase the probe wavelength by 0.05 nm and waited until the stepping motor was fully stopped before we recorded the corresponding background cavity losses again several times. This data collection process was repeated until we reached the end of the 1-nm interval and measured the corresponding background cavity losses. Subsequently, about 4 Torr of water vapor was introduced into the ring-down cavity and the corresponding cavity losses were
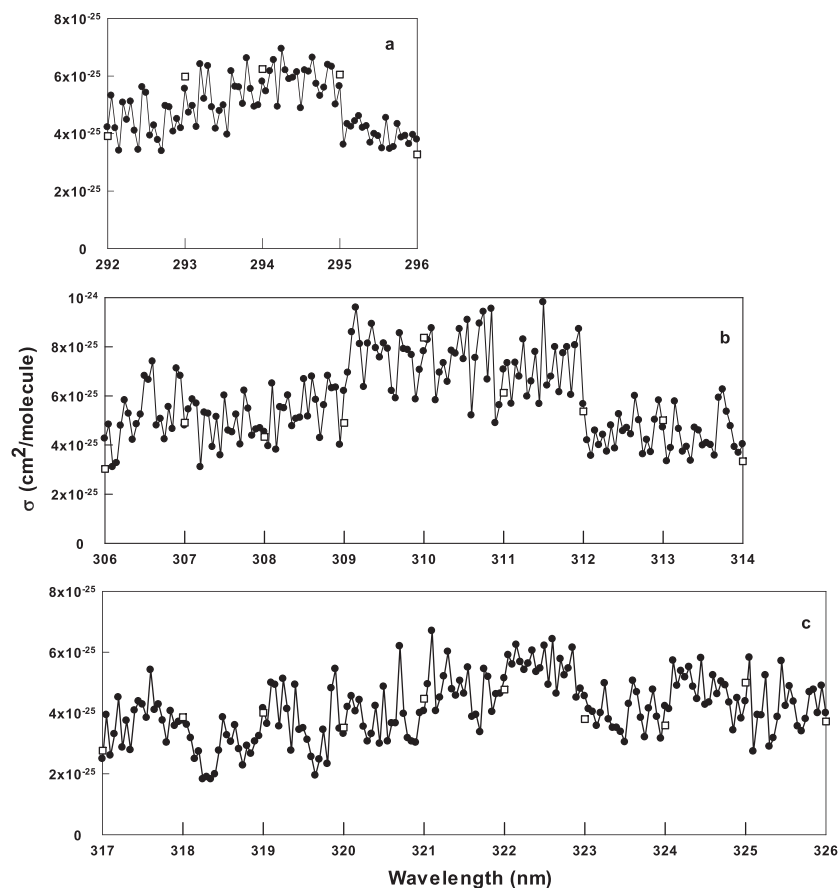
Figure 3. Water vapor absorption cross sections at 0.05-nm intervals (filled circles) and at 1-nm intervals (open squares) over wavelength regions of (a) 292–296 nm, (b) 306–314 nm, and (c) 317–326 nm, where water vapor displays major absorption bands.

determined at 0.05-nm intervals for the entire nanometer. Finally, additional water vapor was introduced into the cavity to reach a final pressure of about 8 Torr, and the cavity losses were again measured at 0.05-nm intervals for the entire nanometer. This data collection procedure allowed us to extract one set of water vapor absorption cross-section data at 0.05 nm intervals for the entire nanometer. We repeated the 0.05-nm interval water vapor cross-section measurements three or more times to ensure the repeatability of the results. Shown in Figure 3 are 0.05-nm interval water vapor absorption cross-section data in the 292- to 296-nm, 306- to 314-nm, and 317- to 326-nm region. It can be seen from Figure 3 that water vapor near-UV absorption displays fine structure in the wavelength region studied. Also displayed in Figure 3 are the 1-nm interval water vapor absorption cross-section data reported in section 3.1.1. There is a good agreement between 1-nm interval water vapor cross-section data and the 0.05-nm interval water vapor cross-section values to within the limit of the combined experimental uncertainty. Estimated relative errors for the water vapor cross-section determination at 0.05-nm intervals are up to about 25–35%.

3.2. Field Evidence for Water Vapor Near-UV Absorption

Surface UV total irradiance (direct + diffuse) spectra collected at Houston, TX, in year 2016 have been reanalyzed to examine water vapor near-UV absorption. The Houston site was chosen, as it is the southernmost U.S. site with a possibility of high water-vapor loadings. The UV flux spectra at the bottom of the atmosphere at different solar angles or AMs were measured daily by a Brewer Mark IV Spectrophotometer from 286.5 to 363 nm at 0.5 nm resolution. Solar irradiance spectra at the top of the atmosphere were approximated using that of reference extraterrestrial solar UV spectrum (Gröbner et al., 2017) convoluted with instrument slit function specified in the instrument manual.

For the direct solar beam, the log ratio of solar irradiance at top of the atmosphere to that at the bottom of the atmosphere gives total optical depth along a path length (AM) of the whole atmosphere at a given wavelength. Atmospheric near-UV absorbing gases such as O_3, SO_2, water vapor, formaldehyde, BrO, and NO_2 as well as aerosol extinction and Rayleigh scattering can affect total optical depth in the near-UV region under clear-sky conditions. Typical concentrations of atmospheric trace gases such as BrO and NO_2 were low and their absorption effects on total optical depth were negligible compared to those of ozone (Chance, 2005) and water vapor. The contribution of SO_2 absorption optical depth to the total was subtracted in the residual analysis to account for possible contamination from long-range transport of volcanic plumes. We used National Aeronautics and Space Administration MERRA-2 (Gelaro et al., 2017) hourly Single-Level Diagnostics ($0.5° \times 0.625°$ resolution) of O_3, SO_2, column water vapor, and surface pressure for the analyses. Absorption spectra of O_3 and SO_2 at the spectrometer resolution were generated by convolving literature absorption spectra of O_3 (Bogumil et al., 2003; Orphal et al., 2016) and SO_2 (Bogumil et al., 2003) with instrument spectral response function represented by Gaussian with width specified by the resolution. By subtracting fitted optical depths of aerosol extinction, Rayleigh scattering, and absorptions by UV absorbing gases such as O_3 and SO_2 from the measured total optical depth, residual optical depth at a given wavelength was obtained. The formula (equation (1)) used in the analysis can be found in section 2. In the presence of diffuse radiation, we used a fitting procedure that considered the vertical distribution of gases and aerosols and avoided the knowledge of exact path lengths. The solar irradiances at the top of the atmosphere (Gröbner et al., 2017) are based on ground-based measurements corrected for atmospheric absorption. Since water vapor absorption in the 300- to 500-nm range was not included in the calculations by Gröbner et al., the top of the atmosphere irradiance spectrum used in the residual analysis could have some uncertainty.

Seventy-nine cloudless days in year 2016 were chosen to evaluate water vapor near-UV absorption in the Houston field UV spectra; 28 days had low water content (column water vapor content (CWVC) < 10 kg/m^2), 28 days had moderate water content (CWVC ~ 10–20 kg/m^2), and 23 days had high water content (CWVC >20 kg/m^2). The residual analysis was made at three different AMs, 2, 2.5, and 3, for all 79 cases. To minimize differences between total column optical depth (derived from TOA and BOA UV spectral measurements) and the sum of optical depths of Rayleigh, aerosol, ozone, and SO_2, all residual spectra were normalized by constraining optical depth values of each residual spectrum in the 340- to 350-nm region where water vapor absorption is minimum. Figure 4a shows the difference between normalized and averaged UV spectra residuals for "dry" (CWVC <10 kg/m^2) and "wet" (CWVC >20 kg/m^2) conditions, at three different AMs, over 306–314 nm range. Differential residual spectra between wet and dry help to remove instrument features from the residual spectra presented in Figure 4a.

In the Houston area, the petrochemical industry releases formaldehyde, which is a UV absorber, to the environment. To discover what contributes to the residual spectra shown in Figure 4a, we plotted the water vapor near-UV absorption spectrum determined in this work (shown in Figure 4b), the formaldehyde near-UV absorption spectrum (Rogers, 1990) shown in Figure 4c, and the ozone near-UV absorption spectrum (Bogumil et al., 2003; Orphal et al., 2016) shown in Figure 4d, over the 306- to 314-nm range. Wet-dry differential residual spectra in the 309- to 312-nm region showed similarity to the reference water vapor near-UV absorption spectrum shown in Figure 4b. This appears to provide additional support for water vapor near-UV absorption. Since water vapor near-UV absorption is weak, we also noticed that not all field residual features match those shown in the laboratory water vapor near-UV absorption spectrum. Some uncertainty in the top of the atmosphere solar irradiance spectrum has been discussed earlier in this section.

We also used the water vapor cross-section data determined in this study and a radiative transfer model (Berk et al., 1989) to calculate the magnitude of wet-dry peak water vapor absorption optical depth for the Houston area, finding it to be about 0.08 over the 309- to 312-nm range compared to the measured peak residual of about 0.17–0.27 (see Figure 4a). Variations in the residual spectra may be affected by uncertainties in the reference extraterrestrial solar UV spectrum and in the instrument spectral response function, both of which were used to model the measured spectra and thus contributed to final residuals displayed in Figure 4a. There was a resemblance between differential residual spectra in the 306- to 307-nm and 313- to 314-nm region and the formaldehyde reference spectrum over the same wavelength intervals.
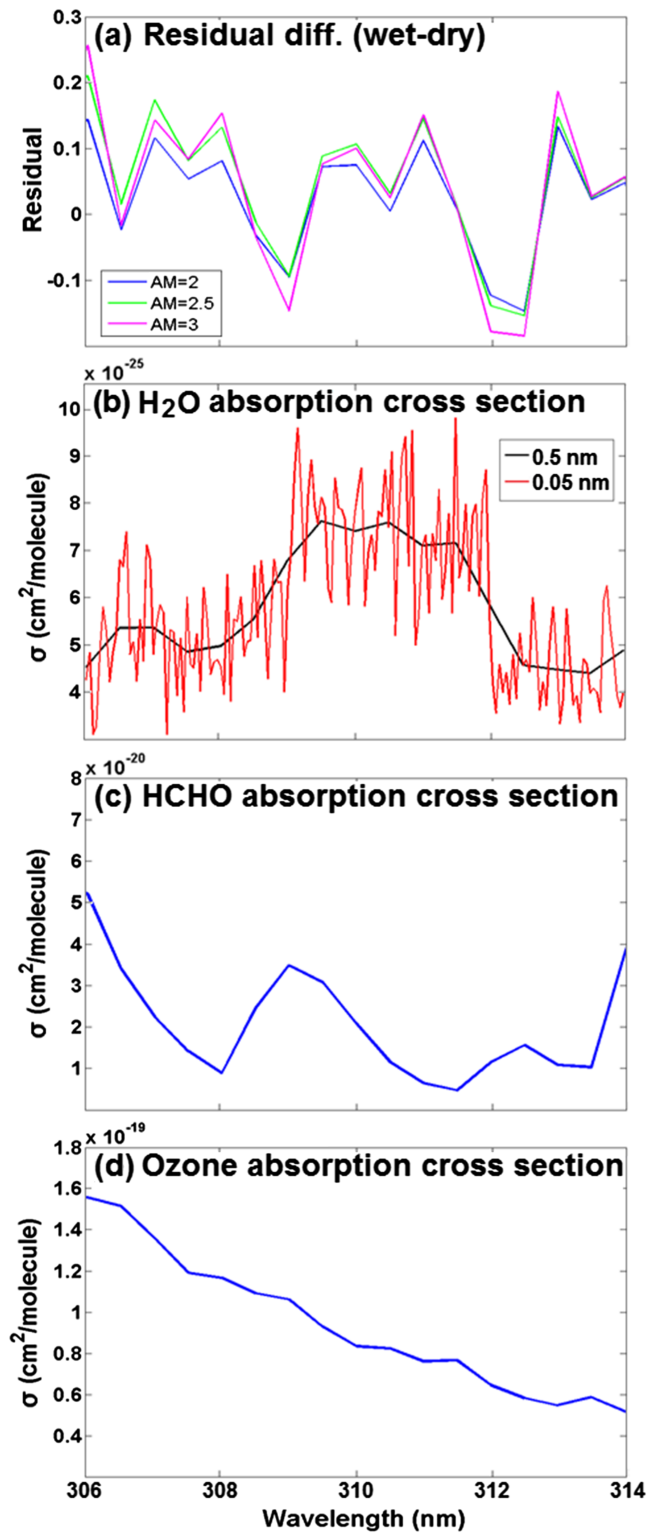
Figure 4. (a) Differential UV residual spectra between "wet" and "dry" atmospheric conditions at Houston, TX, in 2016 over 306- to 314-nm range at three solar air masses; (b) water vapor near-UV absorption spectrum determined in this work over 306- to 314-nm region; and reference UV absorption spectra for (c) formaldehyde and (d) ozone over the same wavelength range.
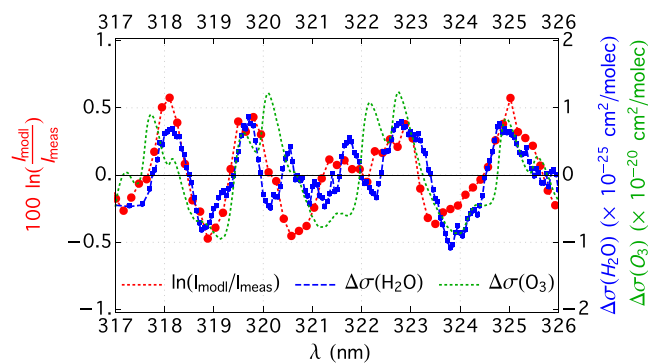
Figure 5. Mean satellite radiance residuals, calculated as the log ratio, $100 \ln (I_{modl}/I_{meas})$, between modeled ($I_{modl}$) and measured ($I_{meas}$) radiances, are overlaid with the differential cross sections of water vapor, $\Delta\sigma$ (H_2O). Differential cross sections were calculated from the difference between the laboratory water vapor cross sections and their least squares fit to a fifth-order polynomial. The laboratory water vapor near-UV spectrum was offset by 0.5 nm (red shift) to compare with satellite residual spectrum, as different absolute wavelength calibration standards were used in OMI versus laboratory water vapor absorption studies (see text for details). The satellite residual spectrum resembles the differential water vapor absorption spectrum. The differential ozone absorption cross sections are plotted in Figure 5 to illustrate the minimal correlation with the satellite residual spectrum.

Therefore, formaldehyde likely contributed to the differential residual spectra in these wavelength intervals. A comparison of differential residual spectra with the ozone reference spectrum further confirmed that ozone absorption features had been mostly removed from these spectra.

Residual analysis of near-UV spectra obtained by satellite was conducted. We compared measured radiance spectra in the 317- to 326-nm range between observations of high and low water vapor loadings. The satellite residuals contained spectral structures composed of atmospheric absorptions (which usually have high-frequency spectral structures) that are not currently included in the retrieval algorithm, scattering from atmospheric particles, reflection from the underlying surface, and instrumental spectral features. Instrumental features remained nearly the same from one measurement to another. The residual originated from scattering and reflection was smooth in wavelength and may be represented by a polynomial of wavelength. The spectral structures associated with atmospheric absorption varied with the column amount and its vertical distribution. To allow for a better comparison with features shown in the laboratory water vapor absorption cross-section spectrum, we removed the smooth part of the residual to emphasize the unaccounted atmospheric absorption structures. Figure 5 shows the average residual difference between observations with high water loading ($\sim$50 kg/m^2) and low water loading ($\sim$10 kg/m^2), overlaid with differential cross sections of water vapor. The water vapor loadings for OMI observations were estimated using MERRA-2 data. The water column amount and its vertical distribution for satellite measurements were not available. The differential cross sections were calculated as the difference between the laboratory water vapor cross-section data over the 317- to 326-nm range and their least squares fit to a fifth-order polynomial. The subtraction of residuals of low water vapor loadings from those of high loadings removed the instrumental features from the residuals, revealing the remainder of the atmospheric absorption structures. Since the retrieval algorithm did not consider the contribution of water vapor near-UV absorption, the retrieved total vertical O_3 columns were higher than the actual values. The remaining satellite residual structures shown in Figure 5 were primarily water vapor absorption structures, as ozone absorption features had already been subtracted, and other trace gases had negligible contributions due to their typical low loadings. The differential ozone absorption cross sections are plotted in Figure 5 to illustrate the small correlation with the satellite residual spectrum. Note that each OMI-measured spectrum was wavelength calibrated using a solar Fraunhofer reference spectrum based on the approach outlined in Casper and Chance (1997). Therefore, the accuracy of wavelength was expected to be better than 0.1 nm for residual spectrum, for which the wavelengths are those in vacuum. The satellite residual spectrum resembled the differential water vapor absorption spectrum. The laboratory water vapor near-UV spectrum was offset by 0.5 nm (red shift), as different absolute wavelength calibration standards were used in OMI versus laboratory water vapor absorption studies. The OMI was based on Casper and Chance (1997), while the wavelength of the third harmonic Nd:YAG-pumped optical parametric oscillator and its frequency-doubled output were calibrated by a field service engineer using a
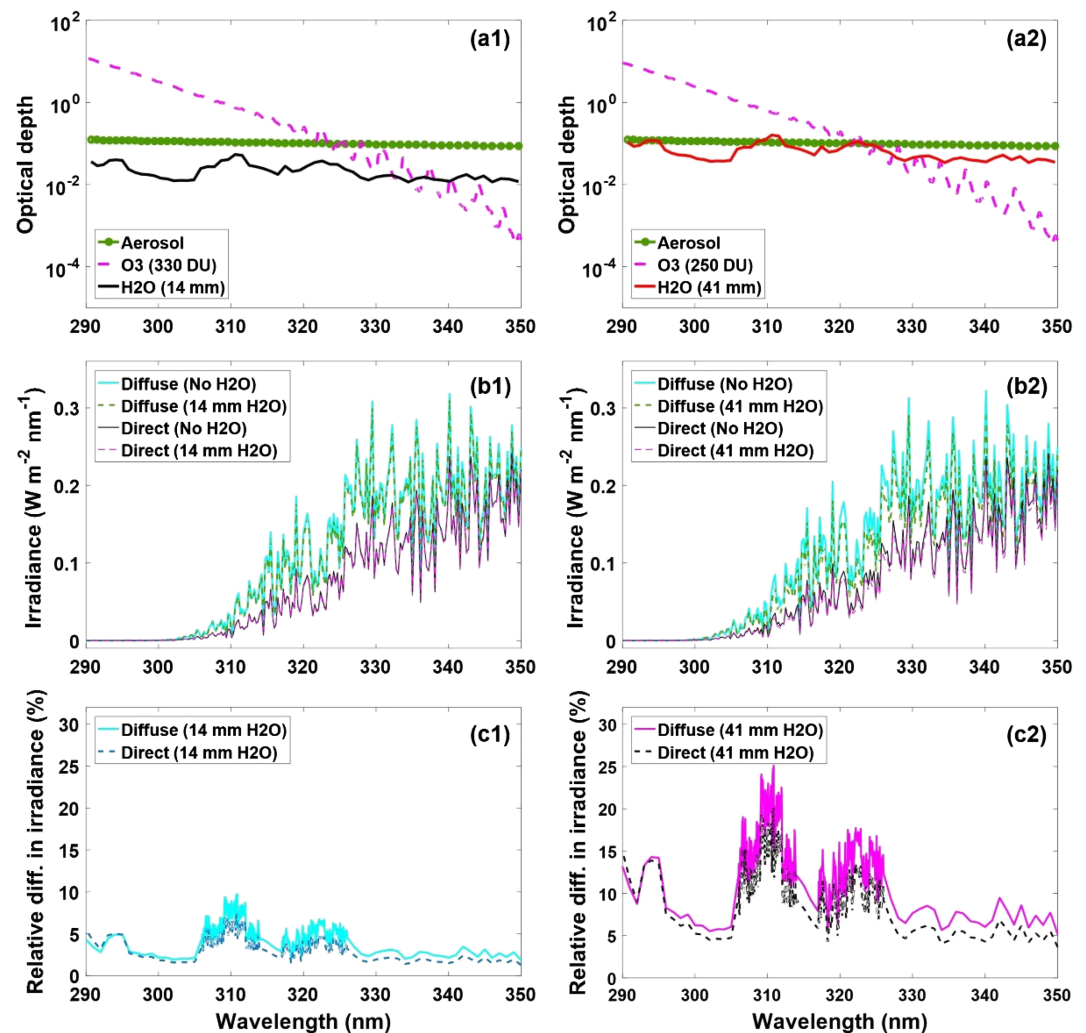
Figure 6. (a) Optical depth spectra of ozone, aerosol, and water vapor for the standard U.S. (a1) and the tropical (a2) atmospheres; (b) simulated surface irradiance spectra with and without water vapor near-UV absorption for direct and diffuse solar radiation for the standard U.S. (b1) and the tropical (b2) atmospheres; (c) the relative difference in the simulated direct and diffuse surface irradiance spectra with and without water vapor near-UV absorption for the standard U.S. (c1) and the tropical (c2) atmospheres.

Lambda meter (the absolute accuracy of wavelength calibration in the near-UV region is estimated about 0.5 nm). It should also be pointed out the absorption feature between 321 and 322 nm was present both in the satellite residual and in the differential water vapor absorption spectrum but not in the ozone absorption spectrum. Thus, satellite results illustrated that water vapor absorption had observable effects on measured Earth View radiance from space. While the structural similarity between the satellite residual spectrum and the laboratory water vapor cross-section spectrum is good overall, we also noticed some differences at 320.5 nm. The satellite findings appear to provide some support for the laboratory wavelength-dependent water vapor near-UV absorption cross sections presented in this paper.

3.3. Atmospheric Impacts Suggested From Radiative Transfer Modeling

We incorporated the water vapor absorption cross-section data reported in this paper into an atmospheric radiative transfer model using the MODTRAN simulation program (Berk et al., 1989) and examined the effect of water vapor near-UV absorption on the modeled radiative flux at the ground level. Input parameters to the MODTRAN program were total ozone of 330 and 250 DU, aerosol optical depth of 0.1 at 320 nm, and condensable water thicknesses of 14 and 41 mm for the standard U.S. and the tropical atmospheres. Figure 6a presents the calculated optical depth spectra of ozone, aerosol, and water vapor for the standard U.S. and the

tropical atmospheres. As seen from Figure 6a, water vapor absorption optical depth changes from being smaller than the ozone Huggins absorption optical depth at wavelengths shorter than 332 nm to exceeding ozone absorption optical depth at wavelengths longer than 341 nm for the standard U.S. atmosphere; water vapor absorption optical depth sometimes exceeds ozone absorption optical depth over the 333- to 340-nm range. Interestingly for the tropical atmosphere, water vapor absorption optical depths are smaller than ozone absorption optical depths at wavelengths shorter than 321 nm; they are comparable to ozone absorption optical depths over the 322- to 331-nm range and larger than ozone absorption optical depths at wavelengths longer than 332 nm. Near-UV absorption by water vapor in the tropical atmosphere will likely affect ozone retrieval based upon spectral fitting in the 322- to 331-nm region. Since near-UV absorption by ozone at 340 nm has been used as a reference channel in the simple ratio ozone retrieval algorithms, tropical water vapor near-UV absorption will significantly affect the accuracy of such retrieved ozone levels. The contribution of aerosol optical depth in the near-UV region is based upon extrapolation of results in the visible range. The modeled tropical water vapor absorption optical depths were larger than those of aerosols in the 309- to 312-nm range. Figure 6b displays simulated surface irradiation spectra, with and without water vapor near-UV absorption, for direct and diffuse solar radiation for the standard U.S. and the tropical atmospheres. In the simulation, the solar zenith angle was set at 55° and the surface albedo was set at 0.03. Figure 6c shows the relative differences with and without water vapor near-UV absorption in the 290- to 350-nm region on the modeled surface irradiance spectra for the standard U.S. and the tropical atmospheres. The relative difference in the simulated direct or diffuse irradiance at the ground level was about 7–9% at 310 nm and about 4–7% at 325 nm for the standard U.S. atmosphere. The relative difference in the simulated direct/diffuse irradiance at the ground level was about 18–23% at 310 nm and about 12–17% at 325 nm for the tropical atmosphere.

Our MODTRAN radiation simulation showed that water vapor absorption in the 290- to 350-nm region can cause significant differences in the modeled direct and diffuse irradiance at the ground level. The estimated energy budget of this previously missing water vapor absorption was about 0.26 W/m^2 for the standard U.S. atmosphere and about 0.76 W/m^2 for the tropical atmosphere. Obtaining realistic predictions about the energy balance of the atmosphere and climate impacts requires not only accounting for projected impacts of anthropogenic perturbations but also accounting for weaker absorptions of naturally occurring dominant atmospheric absorbers that have so far been neglected in the atmospheric radiation models.

4. Conclusions

We constructed a cavity ring-down spectrometer with a bandwidth comparable to those of field UV spectrometers and determined water vapor absorption cross sections at 1-nm intervals in the 290- to 350-nm region. Water vapor displays structured absorption over this range with maximum and minimum cross sections of 8.4×10^{-25} and 1.6×10^{-25} cm^2/molecule. We also measured water vapor absorption cross sections at 0.05 nm intervals surrounding major absorption bands. Here we provide field evidence to support the laboratory water vapor near-UV absorption measurements and present comparisons of the estimated optical depth spectra of ozone with those of water vapor for the standard U.S. and the tropical atmospheres. We found that water vapor near-UV absorption will significantly affect ozone retrieval from UV measurements, particularly in the tropical region. Incorporating water vapor near-UV absorption cross-section data into a radiative transfer model yielded an estimated energy budget (of additional absorption of solar radiation by the atmosphere) of 0.26 W/m^2 for the standard U.S. atmosphere and 0.76 W/m^2 for the tropics. Near-UV solar radiation induces photochemical changes in the troposphere and affects pollutant formation and atmospheric oxidant levels. Thus, water vapor near-UV absorption has impacts not only on atmospheric physics but also on atmospheric chemistry. Results of the current study are expected to facilitate field detection of water vapor near-UV absorption, enable assessment of the radiative and climate impacts of this absorption, and improve ozone retrievals.

References

Atkinson, R., Baulch, D. L., Cox, R. A., Hampson, R. F., Kerr, J. A., Rossi, M. J., & Troe, J. (1997). Evaluated kinetic, photochemical and heterogeneous data for atmospheric chemistry: Supplement V, IUPAC subcommittee on gas kinetic data evaluation for atmospheric chemistry. *Journal of Physical and Chemical Reference Data*, *26*(3), 521–1011. https://doi.org/10.1063/1.556011

Berk, A., Bernstein, L. S., & Robertson, D. C. (1989). MODTRAN: A moderate resolution model for LOWTRAN7 (Rep. AFGL-TR-89-0122), Hanscom AFB, MA: Air Force Geophys. Lab.

Bernath, P. F. (2002). The spectroscopy of water vapour: Experiment, theory and applications. *Physical Chemistry Chemical Physics*, *4*(9), 1501–1509. https://doi.org/10.1039/b200372d

Bogumil, K., Orphal, J., Homann, T., Voigt, S., Spietz, P., Fleischmann, O. C., et al. (2003). Measurements of molecular absorption spectra with the SCIAMACHY pre-flight model: Instrument characterization and reference data for atmospheric remote-sensing in the 230-2380 nm region. *Journal of Photochemistry and Photobiology A: Chemistry*, *157*(2-3), 167–184. https://doi.org/10.1016/S1010-6030(03)00062-5

Casper, C., & Chance, K. (1997). GOME wavelength calibration using solar and atmospheric spectra. In T.-D. Guyenne & D. Danesy (Eds.), *Proc. Third ERS symposium on space at the service of our environment* (Vol. 414, pp. 609–614). Europe Space Agency Special Publication. ISBN 92-9092-656-2,1997.

Chance, K. (2005). Ultraviolet and visible spectroscopy and spaceborne remote sensing of the Earth's atmosphere. *Comptes Rendus Physique*, *6*(8), 836–847. https://doi.org/10.1016/j.crhy.2005.07.010

Choi, S. E., & Light, J. C. (1992). Highly excited vibrational eigenstates of nonlinear triatomic molecules. Application to H_2O. *The Journal of Chemical Physics*, *97*(10), 7031–7054. https://doi.org/10.1063/1.463530

Conway, E. K., Kyuberis, A. A., Polyansky, O. L., Tennyson, J., & Zobov, N. F. (2018). A highly accurate *ab initio* dipole moment surface for the ground electronic state of water vapour for spectra extending into the ultraviolet. *The Journal of Chemical Physics*, *149*(8), 084307. https://doi.org/10.1063/1.5043545

Császár, A. G., Mátyus, E., Szidarovszky, T., Lodi, L., Zobov, N. F., Shirin, S. V., et al. (2010). First-principles prediction and partial characterization of the vibrational states of water up to dissociation. *Journal of Quantitative Spectroscopy and Radiation Transfer*, *111*(9), 1043–1064. https://doi.org/10.1016/j.jqsrt.2010.02.009

Du, J., Huang, L., Min, Q., & Zhu, L. (2013). The influence of water vapor absorption in the 290-350 nm region on solar radiance: Laboratory studies and model simulation. *Geophysical Research Letters*, *40*(17), 4788–4792. https://doi.org/10.1002/grl.50935

Du, J., Huang, L., & Zhu, L. (2013). Absorption cross sections of surface-adsorbed H_2O in the 295-370 nm region and heterogeneous nucleation of H_2O on fused silica surfaces. *The Journal of Physical Chemistry. A*, *117*(36), 8907–8914. https://doi.org/10.1021/jp405573y

Gelaro, R., McCarty, W., Suárez, M. J., Todling, R., Molod, A., Takacs, L., et al. (2017). The Modern-Era Retrospective Analysis For Research And Applications, version 2 (MERRA-2). *Journal of Climate*, *30*(14), 5419–5454. https://doi.org/10.1175/JCLI-D-16-0758.1

Grechko, M., Maksyutenko, P., Zobov, N. F., Shirin, S. V., Polyansky, O. L., Rizzo, T. R., & Boyarkin, O. V. (2008). Collisionally assisted spectroscopy of water from 27000–34000 cm^{-1}. *The Journal of Physical Chemistry. A*, *112*(42), 10,539–10,545. https://doi.org/10.1021/jp805849q

Gröbner, J., Kröger, I., Egli, L., Hülsen, G., Riechelmann, S., & Sperfeld, P. (2017). The high-resolution extraterrestrial solar spectrum (QASUMEFTS) determined from ground-based solar irradiance measurements. *Atmospheric Measurement Techniques*, *10*(9), 3375–3383. https://doi.org/10.5194/amt-10-3375-2017

Hansen, J. E., & Travis, L. D. (1974). Light scattering in planetary atmospheres. *Space Science Reviews*, *16*, 527–610. https://doi.org/10.1007/BF00168069

Houghton, J. T., Ding, Y., Griggs, D. J., Noguer, M., Van der Linden, P. J., Dai, X., et al. (2001). *Climate change 2001: The scientific basis*. Cambridge: Cambridge University Press.

Lampel, J., Pőhler, D., Polyansky, O. L., Kyuberis, A. A., Zobov, N. F., Tennyson, J., et al. (2017). Detection of water vapour absorption around 363 nm in measured atmospheric absorption spectra and its effect on DOAS evaluations. *Atmospheric Chemistry and Physics*, *17*(2), 1271–1295. https://doi.org/10.5194/acp-17-1271-2017

Lampel, J., Pöhler, D., Tschritter, J., Frieß, U., & Platt, U. (2015). On the relative absorption strengths of water vapour in the blue wavelength range. *Atmospheric Measurement Techniques*, *8*(10), 4329–4346. https://doi.org/10.5194/amt-8-4329-2015

Levelt, P. F., van den Oord, G. H. J., Dobber, M. R., Malkki, A., Visser, H., de Vries, J., et al. (2006). The ozone monitoring instrument. *IEEE Transactions on Geoscience and Remote Sensing*, *44*(5), 1093–1101. https://doi.org/10.1109/TGRS.2006.872333

Li, G., & Guo, H. (2001). The vibrational level spectrum of H_2O ($\tilde{X}^1A'$) from the Partridge-Schwenke potential up to the dissociation limit. *Journal of Molecular Spectroscopy*, *210*(1), 90–97. https://doi.org/10.1006/jmsp.2001.8445

Lide, D. R. (2008). *CRC Handbook of Chemistry and Physics* (89th ed.). Boca Raton, FL: CRC Press.

Makogon, M. M., Ponomarev, Y. N., & Tikhomirov, B. A. (2013). The problem of water vapor absorption in the UV spectral range. *Atmospheric and Oceanic Optics*, *26*(1), 45–49. https://doi.org/10.1134/S1024856013010119

Maksyutenko, P., Muenter, J. S., Zobov, N. F., Shirin, S. V., Polyansky, O. L., Rizzo, T. R., & Boyarkin, O. V. (2007). Approaching the full set of energy levels of water. *The Journal of Chemical Physics*, *126*(24), 241101. https://doi.org/10.1063/1.2748751

Min, Q.-L., & Harrison, L. C. (1998). Synthetic spectra for terrestrial ultraviolet from discrete measurements. *Journal of Geophysical Research*, *103*(D14), 17,033–17,039. https://doi.org/10.1029/98JD01452

Mussa, H. Y., & Tennyson, J. (1998). Calculation of the rotation–vibration states of water up to dissociation. *The Journal of Chemical Physics*, *109*(24), ,–10,892. https://doi.org/10.1063/1.476519

Okabe, H. (1978). *Photochemistry of small molecules*. New York, NY: John Wiley and Sons.

O'Keefe, A., & Deacon, D. A. G. (1988). Cavity ring-down optical spectrometer for absorption measurements using pulsed laser sources. *The Review of Scientific Instruments*, *59*(12), 2544–2551. https://doi.org/10.1063/1.1139895

O'Keefe, A., Scherer, J. J., Cooksy, A. L., Sheeks, R., Heath, J., & Saykally, R. J. (1990). Cavity ring down dye laser spectroscopy of jet-cooled metal clusters: Cu_2 and Cu_3. *Chemical Physics Letters*, *172*(3-4), 214–218. https://doi.org/10.1016/0009-2614(90)85390-X

Orphal, J., Staehelin, J., Tamminen, J., Braathen, G., De Backer, M.-R., Bais, A., et al. (2016). Absorption cross-sections of ozone in the ultraviolet and visible spectral regions: Status report 2015. *Journal of Molecular Spectroscopy*, *327*, 105–121. https://doi.org/10.1016/j.jms.2016.07.007

Rogers, J. D. (1990). Supporting information for ultraviolet absorption cross sections and atmospheric photodissociation rate constants of formaldehyde. *The Journal of Physical Chemistry*, *94*(10), 4011–4015. https://doi.org/10.1021/j100373a025

Rothman, L. S., Gordon, I. E., Barbe, A., Chris Benner, D., Bernath, P. F., Birk, M., et al. (2009). The HITRAN 2008 molecular spectroscopic database. *Journal of Quantitative Spectroscopy and Radiation Transfer*, *110*(9-10), 533–572. https://doi.org/10.1016/j.jqsrt.2009.02.013

Sangwan, M., Stockwell, W. R., Stewart, D., & Zhu, L. (2016). Absorption of near UV light by HNO_3/NO_3^- on sapphire surfaces. *The Journal of Physical Chemistry. A*, *120*(18), 2877–2884. https://doi.org/10.1021/acs.jpca.6b01648

Sutton, J. A., & Driscoll, J. F. (2004). Rayleigh scattering cross sections of combustion species at 266, 355, and 532 nm for thermometry applications. *Optics Letters*, *29*(22), 2620–2622. https://doi.org/10.1364/OL.29.002620

Tennyson, J. (2014). Vibration-rotation transition dipoles from first principles. *Journal of Molecular Spectroscopy*, *298*, 1–6. https://doi.org/10.1016/j.jms.2014.01.012

Tennyson, J., Bernath, P. F., Brown, L. R., Campargue, A., Császár, A. G., Daumont, L., et al. (2013). IUPAC critical evaluation of the rotational-vibrational spectra of water vapor. Part III: Energy levels and transition wavenumbers for $H_2^{16}O$. *Journal of Quantitative Spectroscopy & Radiative Transfer*, *117*, 29–58. https://doi.org/10.1016/j.jqsrt.2012.10.002

Wilson, E. M., Wenger, J. C., & Venables, D. S. (2016). Upper limits for absorption by water vapor in the near-uv. *Journal of Quantitative Spectroscopy and Radiation Transfer*, *170*, 194–199. https://doi.org/10.1016/j.jqsrt.2015.11.015

Yang, K., Liu, X., Krotkov, N., Krueger, A. J., & Carn, S. A. (2009). Estimating the altitude of volcanic sulfur dioxide plumes from space borne hyper-spectral UV measurements. *Geophysical Research Letters*, *36*(10), L10803. https://doi.org/10.1029/2009GL038025